An analysis of the steepest descent method to efficiently compute the 3D acoustic single-layer operator in the high-frequency regime

David Gasperini, Hans-Peter Beise, Udo Schröeder, Xavier Antoine, Christophe Geuzaine

An analysis of the steepest descent method to efficiently compute the 3D acoustic single-layer operator in the high-frequency regime

D. Gasperini[*†‡], H-. P. Beise[§], U. Schroeder[*], X. Antoine[†], C. Geuzaine[‡]

Abstract. Using the Cauchy integral theorem, we develop the application of the steepest descent method to efficiently compute the three-dimensional acoustic single-layer integral operator for large wave numbers. Explicit formulas of the splitting points are derived in the one-dimensional case to build suitable complex integration paths. The construction of admissible steepest descent paths is next investigated and some of their properties are stated. Based on these theoretical results, we derive the quadrature scheme of the oscillatory integrals first in dimension one and then extend the methodology to three-dimensional planar triangles. Numerical simulations are finally reported to illustrate the accuracy and efficiency of the proposed approach.

Keywords. high-frequency scattering; acoustic single-layer integral operator; steepest descent method; highly oscillatory integrals

Contents

[*]IEE S.A., Bissen, Luxembourg
[†]Université de Lorraine, CNRS, Inria, IECL, F-54000 Nancy, France
[‡]University of Liège, Montefiore Institute B28, B-4000 Liège, Belgium
[§]Trier University of Applied Sciences, Germany

1 Introduction

We consider the problem of the efficient evaluation of the elementary acoustic single-layer integral operator

$$I_{\mathbf{r},\Delta}(k) = \int_{\Delta} \frac{e^{ik(\|\mathbf{r}-\mathbf{r}'\|+\boldsymbol{\theta}\cdot\mathbf{r}')}}{\|\mathbf{r}-\mathbf{r}'\|} d\mathbf{r}', \tag{1}$$

where $\mathbf{r} \in \mathbb{R}^3$ is an observation point, Δ is a triangle in $\mathbb{R}^3$ and $\boldsymbol{\theta}$ is a given directional unitary vector in $\mathbb{R}^3$. In addition, we set $i := \sqrt{-1}$, and $\|\mathbf{x}\| := \sqrt{\mathbf{x}\cdot\mathbf{x}}$ is the euclidian norm defined through the dot product $\mathbf{x}\cdot\mathbf{y} = \sum_{j=1}^{3} x_j y_j$, for $\mathbf{x}$ and $\mathbf{y}$ in $\mathbb{R}^3$. The problem of the computation of (1) arises for example in the framework of the Physical Optics approximation and integral equations [1, 10, 25, 27], where the real-valued positive constant k is then the wave number. It is well-known that evaluating (1) for large values of k requires a prohibitive computational cost [9, 27], and reducing the complexity is considered as being a challenging and important numerical problem, most particularly when trying to weaken the k-dependence of the computational cost for example by getting a computation of $I_{\mathbf{r},\Delta}(k)$ independent of k. This is the reason why the development of new approximation methods to compute highly oscillatory integrals [11] has received a lot of attention during the last two decades. Among others and without being exhaustive, important achievements in this direction are related to the Levin-type methods [11, 24, 31], the Filon-type discretization technique [2, 11, 13, 14, 19, 20, 22, 23, 31, 33] and the method of steepest descent/stationary phase [3, 4, 6, 17, 27, 28, 29, 30, 32]. Other contributions include e.g. the following references [5, 7, 8, 15, 16, 18, 21, 22, 23]. For completeness, we refer to [11, 15] for a general overview and more references. We focus in this paper on the method of steepest descent [11] for the computation of (1).

Before attacking the full three-dimensional problem, it is standard to start in dimension one. The basic idea of the steepest descent method is then to use the Cauchy Integral Theorem (CIT) to replace the univariate oscillatory integral

$$I(k,a,b) := \int_a^b f(x) e^{ikg(x)} dx \tag{2}$$

by integrals along paths in the complex plane where $e^{ikg(x)}$ is not oscillatory. Throughout this work, f and g are assumed to be real-valued on $[a,b]$ and analytic in a sufficiently large complex domain that contains $[a,b]$. Moreover, f is supposed to be non-oscillatory on $[a,b]$. Now, suppose that an integration is carried out along a path where g has constant real part and positive increasing imaginary part. Then, the key observation is that $e^{ikg(z)}$ is non-oscillatory and exponentially decaying for complex values of $g(z)$, since $e^{ikg(z)} = e^{-k\mathrm{Im}(g(z))} e^{ik\mathrm{Re}(g(z))}$.

Therefore, the steepest descent method is based on building extensions of $[a,b]$ to a complex integration contour which fulfills the previous conditions. Finally, this leads to the following definition of the *steepest descent path*.

Definition 1. *Let us consider the previous notations and let $\mathcal{I} = [0,T[$ be an interval such that $T \in]0,\infty]$. A function $h : \mathcal{I} \to \mathbb{C}$ which satisfies*

$$g(h(t)) = g(h(0)) + it = g(x) + it, \tag{3}$$

for all $t \in \mathcal{I}$, is called [17] a steepest descent path of g on $\mathcal{I}$ with trace $h^* := h(\mathcal{I})$.

In the following, we denote by h_x a steepest descent path starting at $x \in [a,b]$ (*i.e.* $h_x(0) = x$). In the steepest descent method, the goal is to build steepest descent paths originating at the edges of $[a,b]$, and parametrized by a positive real number t, that can be connected by a path $\varphi_{a,b}$ of negligible contribution to the integral. More precisely, we need to find steepest descent paths h_a, h_b, both being defined on $[0,\infty[$, and such that for every $t \geq 0$, there exists a path $\varphi_{a,b}$ defined on $[0,1]$ and two real numbers $t_a, t_b \in [t,\infty[$, with $h_a(t_a) = \varphi_{a,b}(0)$ and $h_b(t_b) = \varphi_{a,b}(1)$, such that the CIT applies on the induced contour and that the following path integral

$$\int_{\varphi_{a,b}} f(z)e^{ikg(z)}dz \to 0$$

as t tends to ∞. Then, the integral (2) can be rewritten as

$$\begin{aligned} I(k,a,b) &= \int_{h_a} f(z)e^{ikg(z)}dz - \int_{h_b} f(z)e^{ikg(z)}dz \\ &= \int_0^\infty h_a'(t)f(h_a(t))e^{ikg(h_a(t))}dt - \int_0^\infty h_b'(t)f(h_b(t))e^{ikg(h_b(t))}dt. \end{aligned} \tag{4}$$

In [15], Huybrechs and Olver present a way to write explicitly the steepest descent paths in the two-dimensional case. However, it is not known whether there exist some extensions of such paths for higher dimensional problems, leading to further investigations to handle multivariate integrals [3, 11, 18, 21, 22, 23]. Nevertheless, it is shown in [18] that the method of steepest descent can be applied to multivariate cubatures by means of nested integrals. In order to apply this method to the integrals of the form (1), the restriction to the corresponding univariate form has to be investigated. Here, it turns out that in general a straightforward application of (4) is not feasible since the validity of the CIT does not hold in all settings, or two paths cannot always be linked by a path of negligible contribution. Such issues are also pointed out in [4]. In the latter work, the author shows that a polar change of variables can circumvent these issues in certain cases. Let us finally remark that recent contributions [26, 27, 28, 29, 30, 32] developed with success the application of the numerical steepest descent method to the Physical Optics in high-frequency electromagnetic scattering, for both linear and quadratic phases.

In this work, we first consider the univariate version of the integral in (1). We identify two types of potential critical points on the integration interval that have to be circumvented by splitting the integration: firstly, stationary points of the phase function, and, secondly, points that give steepest descent path that run into one of the two possible singularities of the integrand in the complex plane. We give some explicit formulas for the determination of these splitting points and show that at most one of them can be present in a given bounded interval. We also provide explicit formulas for the steepest descent path. These paths turn out to differ depending on the location of their starting point with respect to a splitting point and depending on the incident direction of the wave with respect to the integration surface. In all settings, we can prove that paths that start on the same side relative to a splitting point allow the application of the steepest descent method, i.e. they can be connected by a path of negligible contribution to the integral and it is ensured that the Cauchy integral theorem applies on the resulting contour. In the investigation of the steepest descent paths in the context of the univariate case, we also explore the method to determine them by rewriting (3) as an ordinary differential equation. This method is further applicable when no explicit formula for (3) is available and therefore can be considered as an alternative to the Taylor's

series expansion approach given in [6]. For the integration over a two-dimensional surface we follow [18] and write (1) as nested univariate, oscillatory integrals. But in contrast to [18], where the general case is treated, we only consider a fixed type of integral and it turns out that in our case, the oscillatory components in the two perpendicular directions of integration can be decomposed as a product of two oscillatory integrals with a remaining coupled component that only varies slowly in both variables. The latter can hence can be treated by usual numerical methods. Numerical experiments at the end of the paper demonstrate the efficiency and accuracy of the method for univariate and two-dimensional oscillating integrals given by (1).

The paper is organized as follows. In Section 2, we provide the setting and introduce some notations. Section 3 is devoted to the explicit calculation of the splitting points. The construction and properties of admissible steepest descent paths is analyzed in Section 4. Based on these results, we develop the integration technique in Section 5 for the univariate case first, and then for triangular surfaces. Numerical illustrations are provided in Section 6. Section 7 concludes the paper.

2 Settings and notations

Let us consider (1), for a triangle Δ in $\mathbb{R}^3$ and a given unitary vector $\boldsymbol{\theta}$ in $\mathbb{R}^3$. Let us introduce a linear parametrization to map the unit triangle Δ_1 defined by the corners $(0,0)$, $(1,0)$, $(0,1)$ to Δ given by the affine mapping: $\mathbf{x} \mapsto A\mathbf{x} + \mathbf{b}$, with $\mathbf{x} = (x,y)^T$, $A := (A_\ell)_{1\leq\ell\leq 2} \in \mathbb{R}^{3\times 2}$, $A_\ell \in \mathbb{R}^3$ and $\mathbf{b} \in \mathbb{R}^3$. In this case, (1) writes as

$$I_\Delta(k) = |A_1 \times A_2| \int_0^1 \int_0^{1-y} \frac{e^{ik(\|A\mathbf{x}+\mathbf{b}-\mathbf{r}\|+\boldsymbol{\theta}\cdot(A\mathbf{x}+\mathbf{b}))}}{\|A\mathbf{x}+\mathbf{b}-\mathbf{r}\|} dxdy =: |A_1 \times A_2|\, I^1_{\Delta_1}(k), \tag{5}$$

where the index $\mathbf{r}$ in $I_{\mathbf{r},\Delta}(k)$ is avoided to simplify the notations. Let us define $P(x,y) := ||A\mathbf{x}+\mathbf{b}-\mathbf{r}||^2$ as the second-order polynomial with respect to the two variables x and y, which is also denoted by $P(x)$ when y is temporarily frozen. We assume that the observation point $\mathbf{r}$ does not lie in Δ which implies that P only takes positive real values and hence writes as

$$P(x) = c_0(x-c)(x-\overline{c}) = c_0x^2 + c_0|c|^2 - 2c_0x\mathrm{Re}(c), \tag{6}$$

with $c_0 \in [0,\infty[$ and $c \in \mathbb{C}\setminus\mathbb{R}$, where c and $\overline{c}$ are the roots of P. In this section, we only consider the one-dimensional inner integral of $I^1_{\Delta_1}(k)$ for some arbitrary but fixed $y \in [0,1]$, the functions and the coefficients being then y-dependent. The linear part in g is also written as a linear function $x \mapsto \boldsymbol{\theta}\cdot(A\mathbf{x}+\mathbf{b}) =: qx+s$, with real-valued q and s that vary as a function of y. Hence, g is given by

$$g(x) = \sqrt{P(x)} + qx + s \tag{7}$$

and the associated integral is of the following form

$$I(k,y,0,1-y) = \int_0^{1-y} \frac{e^{ikg(x)}}{\sqrt{P(x)}} dx.$$

To keep a certain generality, we rather study integrals over real intervals $[a,b]$ defined by

$$I(k,y,a,b) := \int_a^b \frac{e^{ikg(x)}}{\sqrt{P(x)}} dx. \tag{8}$$

According to Definition 1, we directly see that a steepest descent path $h_x : \mathcal{I} = [0, T[\to \mathbb{C}$, with $T \in]0, \infty]$, starting at $x \in [a, b]$ is defined by the equation

$$g(h_x(t)) = \sqrt{P(h_x(t))} + q h_x(t) + s = \sqrt{P(x)} + qx + s + it, \tag{9}$$

with $h_x(0) = x$. In this early state of the work, $\sqrt{.}$ should denote an analytic continuation of a fixed definition of the square-root at $P(x)$ along the path $P(h_x(t))$ starting at $P(x) = P(h_x(0))$. More precisely, let us define

$$\Pi := \{z \in \mathbb{C} \mid \mathrm{Re}(z) = \mathrm{Re}(c) \quad \text{and} \quad \mathrm{Im}(z) \in]\mathrm{Im}(\overline{c}), \mathrm{Im}(c)[\}$$

and $\Pi^c := \mathrm{Re}(c) + i\,(\mathbb{R} \setminus \Pi)$. One can directly check that the inverse image of $]-\infty, 0]$ under P is Π^c. Hence, if we consider paths that do not intersect Π^c, one can use the main branch of the square-root in (9). We will show how to ensure that the steepest descent paths given in the sequel satisfy the aforementioned condition. As a consequence, the definition of the complex square-root can be fixed to the main branch.

3 Explicit calculation of the splitting points

To compute (8) by the steepest descent method, we have to ensure that two steepest descent paths can be connected by a path of negligible contribution with regard to the integral (see Section 1). To this end, we need to determine the stationary point of g which is a first splitting point. In addition, we guarantee that the steepest descent paths are well-defined and that the closed curve emerging when connecting two such elementary paths does not enclose and/or intersect a root of P defined by (6), which is a singularity of $1/\sqrt{P}$ and hence has to be avoided in (8). Hence, this results in two different classes of splitting points where the integration in (8) must be split. Here, explicit formulas for these points are derived according to the parameters q and c_0 in (6)-(7). In Section 4, we also give explicit formulas for the steepest descent path for each case introduced in Section 2. This provides complete means for the computation of (8) thanks to the steepest descent method.

Let us start with the notion of splitting points.

Definition 2. *In the context of Section 2, there exist two splitting points*

1. *the stationary point c_s of g defined by: $g'(c_s) = 0$,*
2. *and the starting point c_r of a path h_{c_r} passing through a root of P at some point t_{c_r}. Since the real part of g along a steepest descent path is constant, c_r is given by*

$$g(h_{c_r}(0)) = \mathrm{Re}\left(g(h_{c_r}(t_{c_r}))\right) = \mathrm{Re}\left(g(c)\right).$$

These splitting points can be explicitly computed depending on q (see Eq. (7)). A stationary point c_s of the function g is solution to $g'(c_s) = 0$. Considering the explicit definition (7) of g, this is equivalent to solving

$$c_0\,(c_s - \mathrm{Re}(c)) + q\sqrt{P(c_s)} = 0. \tag{10}$$

If $q = 0$, then we obtain: $c_s = \mathrm{Re}(c)$. For $q = \pm\sqrt{c_0}$, we see that the modulus of c_s is infinite. For infinite values of q, we have $c_s = \mathrm{Re}(c) \pm \mathrm{Im}(c)$, and then c_s is bi-valued as solution to (10), taking its values in $\{c, \overline{c}\}$. The equation (10) is equivalent to: $c_s = \mathrm{Re}(c) \pm K_{c_s}$, setting

$$K_{c_s} := \sqrt{\mathrm{Re}(c)^2 + \frac{c_0 \mathrm{Re}(c)^2 - q^2|c|^2}{c_0 - q^2}}.$$

Injecting the above expression in (10) yields: $c_0 K_{c_s} = \pm q\sqrt{P(c_s)}$. If $|q| < \sqrt{c_0}$, then the left hand side is positive. Thus, depending on the sign of q, we conclude for the exact formula of the stationary point. The case $|q| > \sqrt{c_0}$ leads to complex values of c_s and can be treated in a similar way.

The starting point c_r of a path passing through a root of P is defined as solution to

$$g(h_{c_r}(0)) = \mathrm{Re}\left(g(h_{c_r}(t_{c_r}))\right),$$

which is equivalent to solving the equation

$$\sqrt{P(c_r)} + qc_r = \mathrm{Re}(\sqrt{P(c)} + qc).$$

Similarly to c_s, we derive the exact formulas for c_r, depending on q. Let us remark that, if $q = 0$, the term inside the square-root simplifies to $-\mathrm{Im}(c)^2$. Therefore, in this case, c_r is also bi-valued and takes its values in $\{c, \overline{c}\}$. Finally, the results are summarized in Table 1, setting

$$K_{c_r} := \sqrt{\mathrm{Re}(c)^2 + \frac{q^2 \mathrm{Re}(c)^2 - c_0|c|^2}{c_0 - q^2}}.$$

Case		c_s	c_r
$\lvert q\rvert = \infty$		$\{c, \overline{c}\}$	$\mathrm{Re}(c)$
$\lvert q\rvert = 0$		$\mathrm{Re}(c)$	$\{c, \overline{c}\}$
$\lvert q\rvert = \sqrt{c_0}$		$\lvert c_s\rvert = \infty$	$\lvert c_r\rvert = \infty$
$\lvert q\rvert < \sqrt{c_0}$	$q < 0$	$\mathrm{Re}(c) + K_{c_s}$	$\mathrm{Re}(c) + K_{c_r}$
	$q > 0$	$\mathrm{Re}(c) - K_{c_s}$	$\mathrm{Re}(c) - K_{c_r}$
$\lvert q\rvert > \sqrt{c_0}$	$q < 0$	$\mathrm{Re}(c) + K_{c_s}$	$\mathrm{Re}(c) + K_{c_r}$
	$q > 0$	$\mathrm{Re}(c) - K_{c_s}$	$\mathrm{Re}(c) - K_{c_r}$

Table 1: Explicit formulas of the splitting points according to q.

The previous explicit formulas allow to investigate in details the complementary behaviors of c_s and c_r. All the possible cases are described in Figure 1. We can conclude that at most one splitting point exists in a given integration interval $[a; b]$.

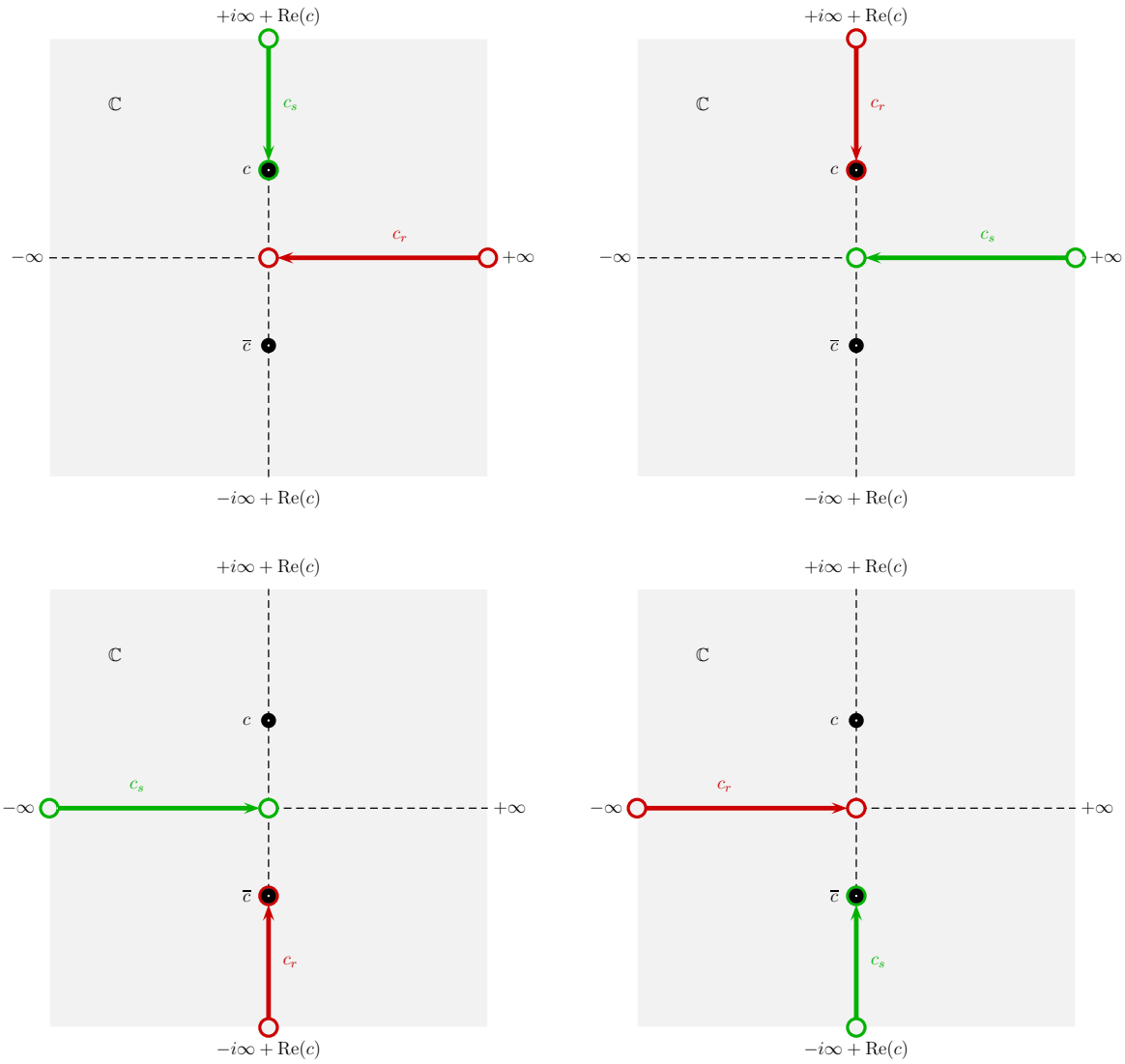

Figure 1: Splitting points of c_r and c_s according to q. Upper left: q starts at $-\sqrt{c_0}$ and tends to $-\infty$. Upper right: q starts at $-\sqrt{c_0}$ and tends to 0. Lower left: q starts at $\sqrt{c_0}$ and tends to 0. Lower right: q starts at $\sqrt{c_0}$ and tends to ∞.

4 Construction and properties of admissible steepest descent paths

4.1 Construction of admissible steepest descent paths

We now introduce the following definition.

Definition 3. *A steepest descent path is called admissible steepest descent path if its starting point belongs to* $\mathbb{R} \setminus \{c_r, c_s\}$.

Let us use (3) to derive the explicit expressions of the admissible steepest descent paths

and its derivatives, which is needed in (4). For a path h_x starting at x, we set:

$$K_x(t) = \sqrt{P(x)} + qx + it,$$

with $t \geq 0$. By the definition (6) giving P, we obtain

$$c_0 h_x(t)^2 + c_0|c|^2 - 2c_0\mathrm{Re}(c)h_x(t) = (K_x(t) - qh_x(t))^2. \tag{11}$$

Let us analyze the different situations according to q. For $q = \sqrt{c_0}$, (11) leads to

$$h_x(t) = \frac{K_x(t)^2 - c_0|c|^2}{2\left(K_x(t)\sqrt{c_0} - c_0\mathrm{Re}(c)\right)}.$$

Similarly, the case $q = -\sqrt{c_0}$ implies that

$$h_x(t) = \frac{K_x(t)^2 - c_0|c|^2}{-2(K_x(t)\sqrt{c_0} + c_0\mathrm{Re}(c))}.$$

Now, let us consider the complementary case $|q| \neq \sqrt{c_0}$. Eq. (11) leads to

$$h_x(t) = K^1_{h_x} \pm K^2_{h_x}, \tag{12}$$

with $t \geq 0$, setting

$$K^1_{h_x} := \frac{c_0\mathrm{Re}(c) - qK_x(t)}{c_0 - q^2}, \qquad K^2_{h_x} := \sqrt{\frac{K_x(t)^2 - c_0|c|^2}{c_0 - q^2} - \left(\frac{qK_x(t) - c_0\mathrm{Re}(c)}{c_0 - q^2}\right)^2}.$$

Let us assume, without loss of generality, that $\mathrm{Re}(c) = 0$. Indeed, if not, it only consists in a shift of the system. Then, formula (12) becomes

$$h_x(t) = \frac{-qK_x(t)}{c_0 - q^2} \pm \frac{\sqrt{c_0}}{|c_0 - q^2|}\sqrt{\Phi(t)}, \tag{13}$$

with $\Phi(t) = \mu - t^2 + 2it\nu$, $\nu = \sqrt{P(x)} + xq$ and $\mu = \nu^2 - |c|^2(c_0 - q^2)$. Using these notations, it appears that $\mathrm{Re}(\Phi(t)) = \mu - t^2$ is decreasing and that $\mathrm{Im}(\Phi(t)) = 2t\nu$ is increasing with respect to t. We observe that the real part of the first term of (13) is constant. Hence, the variations of $\mathrm{Re}(h_x(t))$ are given by those of $\mathrm{Re}(\sqrt{\Phi})$. A direct analysis of $\sqrt{\Phi}$ shows that

- $|\mathrm{Im}(\sqrt{\Phi})|$ is increasing,
- if $|q| < \sqrt{c_0}$, then $\mathrm{Re}(\sqrt{\Phi})$ is increasing,
- if $|q| > \sqrt{c_0}$, $\mathrm{Re}(\sqrt{\Phi})$ decays.

The term $\sqrt{\Phi(t)}$ writes

$$\sqrt{\Phi(t)} = \pm\sqrt{\frac{1}{2}\left(|\Phi| + \mathrm{Re}(\Phi)\right)} \pm i\sqrt{\frac{1}{2}\left(|\Phi| - \mathrm{Re}(\Phi)\right)}.$$

Amongst the four possible combinations of signs, the main branch of the complex square-root only provides those with a positive real part, i.e. $(+,+)$ and $(+,-)$. In the case $|q| > \sqrt{c_0}$, we

know that the contribution of $\sqrt{\Phi}$ to the real part of the path is still decreasing and positive. Let us recall that, for $q > 0$, all the paths have a positive imaginary part and an increasing real part. To respect these conditions, we must subtract the decaying real part, and then choose the operator $-$. Similarly, for $q < 0$, we choose the operator $+$. The case $|q| < \sqrt{c_0}$ can be investigated in a similar way. The situation $q = 0$ follows exactly the same procedure, depending on the position of the starting point with respect to c_s. Finally, the formulas for the derivatives of the paths are directly obtained by differentiating with respect to t.

We summarize the results in Table 2 for a path h_x starting at $x \in \mathbb{R}$, according to q, where

$$\rho^{\pm} := \frac{1}{c_0 - q^2}\left(-qK_x^{'}(t) \pm \frac{2K_x(t)K_x^{'}(t) - 2\left(qK_x(t) - c_0\mathrm{Re}(c)\right)\frac{qK_x^{'}(t)}{c_0 - q^2}}{2K_{h_x}^2}\right)$$

and

$$\tau^{\pm} := \frac{K_x^{'}(t)K_x(t)^2\sqrt{c_0} \mp 2K_x^{'}(t)K_x(t)c_0\mathrm{Re}(c) + K_x^{'}(t)c_0^{3/2}|c|^2}{\pm 2\left(K_x(t)\sqrt{c_0} \mp c_0\mathrm{Re}(c)\right)^2}.$$

Case		$h_x(t)$	$h_x'(t)$
$q = \pm\sqrt{c_0}$		$\dfrac{K_x(t)^2 - c_0\lvert c\rvert^2}{\pm 2(K_x(t)\sqrt{c_0} \mp c_0\mathrm{Re}(c))}$	$\tau^{\pm}$
$\lvert q\rvert < \sqrt{c_0}$	$x < c_s$	$K_{h_x}^1 - K_{h_x}^2$	ρ^-
	$x > c_s$	$K_{h_x}^1 + K_{h_x}^2$	ρ^+
$\lvert q\rvert > \sqrt{c_0}$	$q < 0$	$K_{h_x}^1 + K_{h_x}^2$	ρ^+
	$q > 0$	$K_{h_x}^1 - K_{h_x}^2$	ρ^-

Table 2: Explicit formulas for h_x and h_x' according to q and x.

4.2 ODE reformulation and properties of the admissible steepest descent paths

Let us start with the following proposition.

Proposition 1. *Let $\chi := \{x \in \mathbb{C} \mid g'(x) = 0\}$. Then, the following results hold*

i) If g is a general phase function as introduced in Section 1, i.e. g is analytic in some sufficiently large domain that contains $[a, b]$, and if $x \in [a, b] \setminus \chi$, then system (3) admits locally a unique steepest descent path as solution. The solution can be determined by

solving the initial value problem

$$\begin{cases} h_x'(t)g'(h_x(t)) = i, & t > 0, \\ h_x(0) = x. \end{cases} \tag{14}$$

ii) If g is specified as in (7) and $x \in \chi$, then g is locally not invertible at x and (3) admits some non-unique solutions originating from x.

Proof. Let us start with i). For fixed $x \in [a,b]$ and $t \in [0,\infty[$, the initial value problem is immediately derived from (3). Since g is supposed to be analytic on some domain $X \subset \mathbb{C}$ containing $[a,b]$ and non-constant since we assume that there exists $x \in [a,b]\backslash\chi$, χ is a discrete set and $\mathcal{F}(t,y) \mapsto ig'(y)^{-1}$ is smooth in the open set $X \setminus \chi$. In particular, its derivative with respect to h_x is continuous on $[a,b]\backslash\chi$. Hence, according to the Cauchy-Kovalevskaya theorem [12] there exists some open interval of $[0,\infty[$ on which the problem admits a unique analytic solution, hence of class $\mathcal{C}^1$, and continuous at 0.

Let us now focus on ii). This statement is given in [15]. However, it can be directly checked in our particular framework with (14). If $h_x(t) \notin \chi$ for all $t \geq 0$ and using (6), (7) gives

$$\begin{cases} h_x'(t) = \dfrac{i}{g'(h_x(t))} = \dfrac{i\sqrt{P(h_x(t))}}{c_0(h_x(t) - \mathrm{Re}(c)) + q\sqrt{P(h_x(t))}}, \\ h_x(0) = x. \end{cases} \tag{15}$$

Here, at some $x \in \chi$ there are exactly two solutions: one path in the upper complex half plane and another one in the lower half plane. □

Solving the nonlinear system (3) amounts to the computation of the inverse function g^{-1} which might be a difficult task in general (and impossible at $x \in \chi$). However, in many cases only a rough approximation of the exact path is needed which might be accomplished by solving (14).

Before formulating some important properties regarding the trace of steepest descent path, let us recall the following notations: $\Pi := \{z \in \Gamma_c \mid \mathrm{Im}(z) \in]\mathrm{Im}(\bar{c}), \mathrm{Im}(c)[\ \}$ and $\Pi^c = \Gamma_c \setminus \Pi$, with $\Gamma_c := \mathrm{Re}(c) + i\mathbb{R}$. The value of q and the position of the starting point on the real axis are the two fundamental criteria that determine the compatibility between paths to apply in the steepest descent method. This fact is illustrated by Figure 2.

Theorem 1 below provides a rigorous justification of the behavior of the steepest descent paths which is observed in Figure 2. The proof needs the following proposition.

Proposition 2. *Two admissible steepest descent paths can never intersect.*

Proof. The result is a consequence of the fact that g must have a constant real part when applied along paths of the steepest descent. □

We can now prove the following Theorem.

Theorem 1. *In the setting introduced in Section 2, we consider an admissible steepest decent path h_x and the parameter q. We denote by c_{sr} a real number which equals the (real) splitting point, when it exists, and we define $e := \mathrm{Re}(h_x(0)) - \mathrm{Re}(c_{sr})$. Then, the following results hold*

i) The absolute value of $\mathrm{Im}(h_x(t))$ tends to infinity as $t \to \infty$.

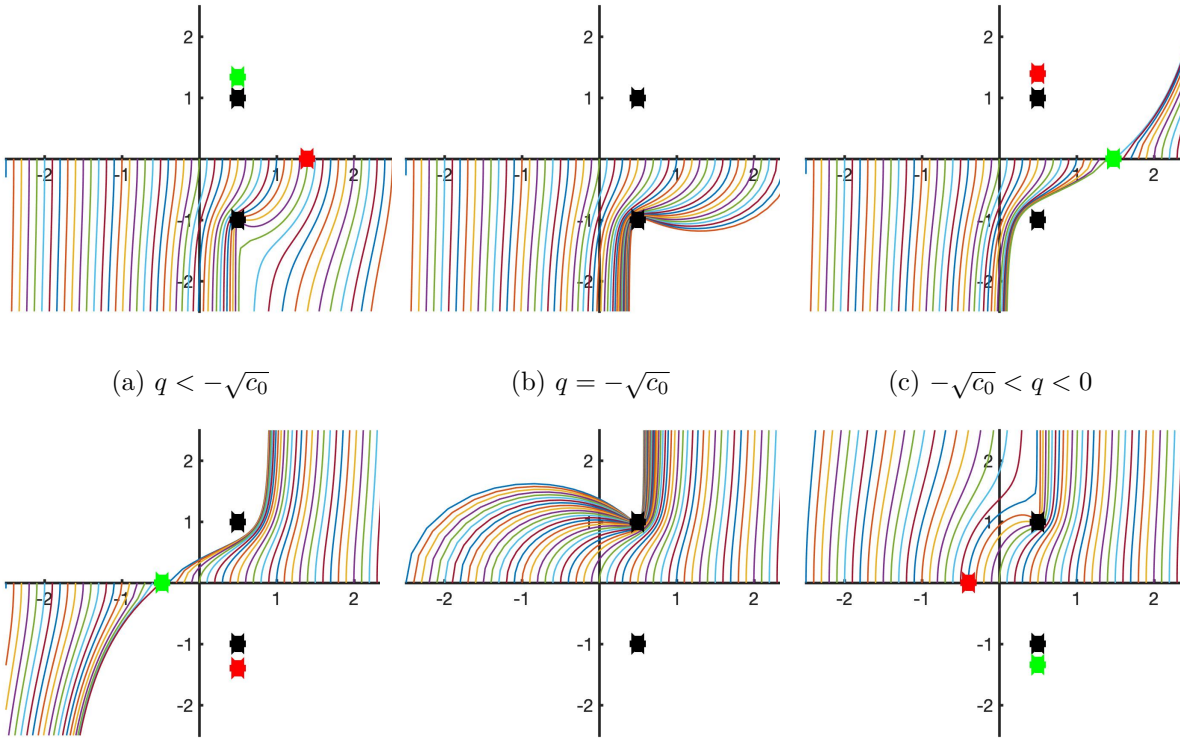

(a) $q < -\sqrt{c_0}$ (b) $q = -\sqrt{c_0}$ (c) $-\sqrt{c_0} < q < 0$

(d) $0 < q < \sqrt{c_0}$ (e) $q = \sqrt{c_0}$ (f) $\sqrt{c_0} < q$

Figure 2: Steepest descent paths for several starting points in $[-2.5, 2.5]$ for $q = -1.5, -1, -0.7, 0.7, 1, 1.5$ in (a), (b), (c), (d), (e), (f), respectively, and throughout $c_0 = 1$, $c = 0.5 + i$, $\overline{c} = 0.5 - i$. The red dot designates c_r, the green one is c_s and the black ones refer to c, $\overline{c}$.

ii) *The trace h_x^* does not intersect Π^c.*

iii) $\mathrm{Re}(h_x)$ *is a monotonous function of t: it is increasing when $q \geq \sqrt{c_0}$ or for $x > c_s$. Otherwise, it is a decaying function.*

iv) *If* $\mid q \mid \geq \sqrt{c_0}$, *then* $\mathrm{sign}(\mathrm{Im}(h_x(t))) = \mathrm{sign}(q)$. *Otherwise, we have:* $\mathrm{sign}(\mathrm{Im}(h_x(t))) = \mathrm{sign}(e)$.

v) *If* $\mid q \mid = \sqrt{c_0}$, *then there exists $T_0 \geq 0$ such that for all $t \geq T_0$, we have*

$$\mathrm{sign}(q)\mathrm{Re}(h_x(t)) > \mathrm{sign}(q)\mathrm{Re}(c).$$

Otherwise, for all $t \geq T_0$, for some $T_0 \geq 0$, we have: $\mathrm{sign}(e)\mathrm{Re}(h_x(t)) > \mathrm{sign}(e)\mathrm{Re}(c)$.

Proof. Let us prove the different points.

i) The imaginary part of the phase function g applied to h is bounded in domains with bounded imaginary part. Hence, since h is a steepest descent path, (3) holds and by contraposition $\mathrm{Im}(h(t))$ tends to infinity as $t \to \infty$.

ii) Let us show the statement for the case $\mid q \mid > \sqrt{c_0}$ (see Figure 2 to sketch the idea), the other situations can be treated in a similar way. We consider a path h_{c_r} which satisfies Definition 1 but starting at c_r. Such a path reaches the root of P of positive imaginary value at time t_{c_r}, and then continuously and monotonously describes $\Pi^c_+ := \{z \in \Pi^c \mid \mathrm{Im}(z) > 0\}$ (this is deduced by the explicit formulations which also show that for all $t > t_{c_r}$, the derivative of such a path is purely imaginary, with positive absolute value). In addition, h_{c_r} is not an admissible steepest descent path, but it however satisfies properties used in the proof of Proposition 2. Hence, it splits the upper complex half plane in two open and disjoint domains. This is the reason why the trace h_x of some arbitrary steepest descent path starting at $x \in \mathbb{R} \setminus \{c_s, c_r\}$ never intersects Π^c_+.

iii) The property is a consequence of the explicit formulation of the paths.

iv) From (15), it turns out that the derivative of a path at its starting point is purely imaginary, and its sign depends on the position of the starting point and the value of q, as stated in iii). Furthermore, Proposition 2 ensures that no steepest descent path crosses the real axis. Hence, the sign of the imaginary value of the steepest descent paths remains constant.

v) It is a direct consequence of points i)-iv), together with Proposition 2. □

5 Integration

5.1 Integration in one-dimension

We show in Theorem 2 below that two admissible steepest descent paths starting from points located on the same side of c_r and c_s can be connected in such a way that the steepest descent method is applicable. Otherwise, this is usually not true. Thus, the application of the steepest descent method on an interval $[a, b]$ that contains c_s or c_r requires a decomposition of the integral in three terms

$$I(k, y, a, b) = I(k, y, a, a_1) + I(k, y, a_1, b_1) + I(k, y, b_1, b), \tag{16}$$

with $[a_1, b_1]$ a small interval that contains either c_s or c_r. The integral $I(k, y, a_1, b_1)$ over the segment $[a_1, b_1]$ can be computed by standard quadrature rules.

The previous theorem ensures that if the integration in (8) is split at c_s and c_r as depicted in Figure 2, then the resulting closed curve, composed by real interval, admissible steepest descent path and linear connection between the two (for given finite argument t) fulfill the assumption of the CIT. Together with the following result, this proves the applicability of the steepest descent method to (8) provided that c_s and c_r are considered accordingly.

Theorem 2. *Let $a < b$ be on the same side of a splitting point, and h_a and h_b be two admissible steepest descent paths, such that for some $t_0 \geq 0$*

$$\min(\mathrm{Re}(h_a(t)), \mathrm{Re}(h_b(t))) > \mathrm{Re}(c) \text{ or } \max(\mathrm{Re}(h_a(t)), \mathrm{Re}(h_b(t))) < \mathrm{Re}(c)$$

when $t > t_0$. Then, the following equality holds

$$\int_a^b \frac{e^{ikg(x)}}{\sqrt{P(x)}} \mathrm{d}x = \int_0^\infty \frac{e^{ikg(h_a(t))}}{\sqrt{P(h_a(t))}} h_a'(t)\, \mathrm{d}t - \int_0^\infty \frac{e^{ikg(h_b(t))}}{\sqrt{P(h_b(t))}} h_b'(t)\, \mathrm{d}t. \tag{17}$$

Proof. From Theorem 1 i), one gets that both $\mathrm{Im}(h_a(t))$ and $\mathrm{Im}(h_b(t))$ either tend to $+\infty$ or $-\infty$ as $t \to \infty$. Thus, for an arbitrary large $M > 0$, we can find $t_1, t_2 > t_0$ such that $\mathrm{Im}(h_a(t_1)) = \mathrm{Im}(h_b(t_2))$ and $|\mathrm{Im}(h_a(t_1))| > M$. Let φ_M denotes the path that describes the linear segment connecting $h_a(t_1)$ and $h_b(t_2)$ and let ϕ_M be the closed path along $[a, b]$, h_b, φ_M and h_a. Theorem 1 i), entails that neither h_a nor h_b intersect Γ_c. This condition and the assumption of Theorem 2 ensure that $\frac{e^{ikg(z)}}{\sqrt{P(z)}}$ is holomorphic in an open neighborhood of the interior of ϕ_M and hence by the CIT one gets

$$\int_{\phi_M} \frac{e^{ikg(z)}}{\sqrt{P(z)}} \mathrm{d}z = 0. \tag{18}$$

By construction, φ_M is a line segment with constant imaginary part that is entirely located in either $\{z : \mathrm{Re}(z) < \mathrm{Re}(c)\}$ or $\{z : \mathrm{Re}(z) > \mathrm{Re}(c)\}$. Therefore, one easily verifies that the imaginary part of the phase function g takes its maximum value over φ_M at $h_a(t_1)$ or $h_b(t_2)$. As M can be arbitrary large, this implies that the integral over φ_M tends to zero as $t_1, t_2 \to \infty$. Hence, we proved (17). □

Finally, we obtain that $I(k, y, a, b)$ writes

$$\begin{aligned} I(k,y,a,b) &= \int_a^b f(x) e^{ik(g(x))} \mathrm{d}x = \int_{h_a} \frac{e^{ik\left(\sqrt{P(z)}+zq+s\right)}}{\sqrt{P(z)}} \mathrm{d}z - \int_{h_b} \frac{e^{ik\left(\sqrt{P(z)}+zq+s\right)}}{\sqrt{P(z)}} \mathrm{d}z \\ &= \int_0^\infty \frac{e^{ik\left(\sqrt{P(h_a(t))}+h_a(t)q+s\right)}}{\sqrt{P(h_a(t))}} h_a'(t) \mathrm{d}t - \int_0^\infty \frac{e^{ik\left(\sqrt{P(h_b(t))}+h_b(t)q+s\right)}}{\sqrt{P(h_b(t))}} h_b'(t) \mathrm{d}t \\ &= \int_0^\infty e^{ik\left(\sqrt{P(a)}+aq+s\right)} \frac{e^{-kt}}{\sqrt{P(h_a(t))}} h_a'(t) \mathrm{d}t - \int_0^\infty e^{ik\left(\sqrt{P(b)}+bq+s\right)} \frac{e^{kt}}{\sqrt{P(h_b(t))}} h_b'(t) \mathrm{d}t. \end{aligned}$$

5.2 Integration over triangular surfaces

In this section, we move from the univariate integral in (8) to our initial objective, namely the numerical computation of the two-dimensional surface integral in (1). In [18], the authors provide theoretical results that deduce the application of the steepest descent method for multivariate oscillatory integrals for general functions that are analytic in some open complex neighbourhood of the domain of integration under some additional conditions [18, Theorem 4.5]. Based on a Filon type approach, the authors also derive a general cubature rule for those cases and quantify the corresponding accuracy. This method requires the computation of nested steepest descent path integrals with integrands that consist of a product of a multivariate monomial times a decaying term of the shape $e^{-k\sum p_j}$, where the p_j mean the non-negative integration variables, times the derivatives of the path functions. In this way, the non-oscillatory factor in the original integral vanishes in these nested path integrals and is instead taken into account in form of a truncated Taylor series [18, Section 5].

Here, we propose to handle the two dimensional integral in a different way. The crucial observation is that in our case, the oscillatory term in the outer integration variable of the nested two-dimensional integral can be factored out from the inner integral. As a consequence, we can avoid nested path integrals and the integration of the non-oscillatory part can be treated by means of usual numerical integration methods.

Let us decompose Δ_1 in n_y layers parallel to the x-axis and compute the value of the integral on each layer in the formula below. We assume that none of the layers in Δ_1 contain

a splitting point. Otherwise, the formula has to be split according to well-chosen sub-areas. The dependency of each parameter on the variables x and y is now specified, and we set $s := s_x + s_y$. Then, we have

$$\begin{aligned} I^1_{\Delta_1}(k) &= \int_0^1 \int_0^{1-y} \frac{e^{ik\left(\sqrt{P(x,y)}+q_y x+q_x y+s\right)}}{\sqrt{P(x,y)}}\mathrm{d}x\mathrm{d}y \\ &= \int_0^1 I(k,y,0,1-y)\mathrm{d}y \\ &= \sum_{j=1}^{n_y}\int_{y_{j-1}}^{y_j}\left[\int_0^\infty \frac{e^{-kt+ik\left(\sqrt{P(0,y)}+q_x y+s\right)}}{\sqrt{P(h_0(t),y)}}h_0'(t)\mathrm{d}t\right. \\ &\quad \left. -\int_0^\infty \frac{e^{-kt+ik\left(\sqrt{P(1-y,y)}+q_y(1-y)+q_x y+s\right)}}{\sqrt{P(h_{1-y}(t),y)}}h_{1-y}'(t)\mathrm{d}t\right]\mathrm{d}y \\ &= \sum_{j=1}^{n_y}\int_{y_{j-1}}^{y_j}\left[e^{ik\left(\sqrt{P(0,y)}+q_x y+s\right)}\int_0^\infty \frac{e^{-kt}}{\sqrt{P(h_0(t),y)}}h_0'(t)\mathrm{d}t\right. \\ &\quad \left. -e^{ik\left(\sqrt{P(1-y,y)}+q_y(1-y)+q_x y+s\right)}\int_0^\infty \frac{e^{-kt}}{\sqrt{P(h_{1-y}(t),y)}}h_{1-y}'(t)\mathrm{d}t\right]\mathrm{d}y. \end{aligned} \tag{19}$$

To each value y in $[0,1]$ corresponds a unique layer of Δ_1. Then, for $y \in [0,1]$ and $a \in [0, 1-y]$, we define the path $h_{a,y}$ as the steepest descent path starting at (a,y) (i.e. the starting point a on the layer y). The dependency of a with respect to y is implicit. We remark now that the function

$$\Lambda_a : y \mapsto \int_0^\infty \frac{e^{-kt}}{\sqrt{P(h_{a(y)}(t),y)}}h_{a(y)}'(t)\mathrm{d}t \tag{20}$$

is smooth and does not vary significantly. Hence it might be approximated by constant functions on elementary intervals $[y_{j-1}, y_j]$ composing $[0,1]$. This behaviour is illustrated for the configuration

$$A = \begin{pmatrix} 0 & 0 \\ 1 & 0 \\ 0 & 1 \end{pmatrix} \qquad \mathbf{b} = \begin{pmatrix} 0 \\ 0 \\ 0 \end{pmatrix} \qquad \mathbf{r} = \begin{pmatrix} 0.3 \\ 0.5 \\ 0 \end{pmatrix} \qquad \boldsymbol{\theta} = \begin{pmatrix} 1 \\ 2 \\ 0 \end{pmatrix} \tag{21}$$

in Figure 3.

This is the crucial point in the numerical calculation of $I_{\Delta_1}(k)$. We now formalize this observation, showing that, under reasonable assumptions, the deviation of Λ in y is controlled by a Lipschitz constant which is independent of any oscillating term in the variable y. For all x, y in $\mathbb{C}$, we define

$$\mu : (x,y) \mapsto \frac{1}{\sqrt{P(x,y)}},$$

which is $\mathcal{C}^\infty$ on $\mathcal{D}_\mu := \{(x,y) \in \mathbb{C}^2 / P(x,y) \notin]-\infty, 0]\}$. It is clear that on every compact set $K \subset \mathcal{D}_\mu$, the function μ is Lipschitz continuous with some fixed constant $L := L_K > 0$. Let us remind that we have some layers free of any splitting point, implying that we have paths along which the integrand is well-defined.

Then, we have the following theorem which confirms that the computational cost of the method only depends on the discretization but not on the wave number k.

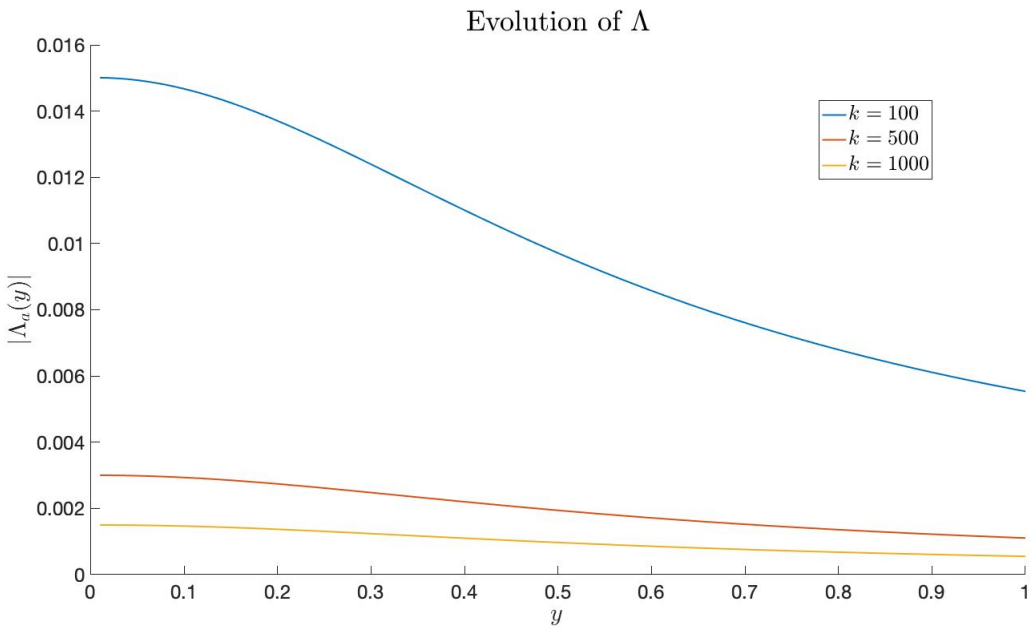

Figure 3: Variation of $|\Lambda_a|$ for the configuration given by (21) with a resolution of 10^{-2} in the y-direction in (19).

Theorem 3. *For each arbitrary interval $[y_{j-1}, y_j]$, there exists a positive constant $C^{\Lambda}_{y_j,y_{j-1}}$ which does not depend on the oscillatory term e^{ik} and such that*

$$\left|\Lambda_a(y) - \Lambda_a(y_{m_j})\right| \quad \leq \quad C^{\Lambda}_{y_j,y_{j-1}} \left|y_j - y_{j-1}\right|,$$

with $y_{m_j} := \frac{y_j + y_{j-1}}{2}$.

Proof. We consider y varying on the fixed interval $[y_{j-1}, y_j]$. Thus, for all $t \in \mathbb{R}$ and $a \in [0, 1-y]$, the Lipschitz condition above implies

$$|\mu(h_{a,y}(t), y) - \mu(h_{a,y_{m_j}}(t), y_{m_j})| \leq L \left\| \begin{pmatrix} h_{a,y}(t) \\ y \end{pmatrix} - \begin{pmatrix} h_{a,y_{m_j}}(t) \\ y_{m_j} \end{pmatrix} \right\|. \tag{22}$$

The exponential decay related to e^{-kt}, for $t \geq 0$, guarantees that there exists a threshold parameter $T_0 > 0$ such that

$$\Lambda_a \approx \int_0^{T_0} \frac{e^{-kt}}{\sqrt{P(h_{a,y}(t), y)}} h'_{a,y}(t) \mathrm{d}t,$$

where $\approx$ formally means that the equality holds up to an *a priori* numerically negligible term. The continuity of the paths and their derivatives with respect to y can be deduced from the explicit formulations in Table 2. Hence, by compactness arguments, there exist strictly positive values M_h and $M_{h'}$ such that one obtains

$$\max_{y \in [y_{j-1}, y_j], t \in [0, T_0]} \left| h_{a,y}(t) - h_{a,y_{m_j}}(t) \right| \leq M_h \left| y_j - y_{j-1} \right| \tag{23}$$

and

$$\max_{y\in[y_{j-1},y_j],t\in[0,T_0]} \left|h'_{a,y}(t) - h'_{a,y_{m_j}}(t)\right| \leq M_{h'} \left|y_j - y_{j-1}\right|. \tag{24}$$

Let $y \in [y_{j_1}, y_j]$ and $t \in [0, T_0]$. Then, (22) and (23) lead to the sequence of inequalities

$$\begin{aligned} |\mu(h_{a,y}(t), y) - \mu(h_{a,y_{m_j}}(t), y_{m_j})| &\leq L\left(\left(h_{a,y}(t) - h_{a,y_{m_j}}(t)\right)^2 + \left(y - y_{m_j}\right)^2\right)^{\frac{1}{2}} \\ &\leq L\left(M_h^2\left(y_j - y_{j-1}\right)^2 + \left(\frac{y_j - y_{j-1}}{2}\right)^2\right)^{\frac{1}{2}} \\ &= L\left|y_j - y_{j-1}\right|\left(M_h^2 + \frac{1}{4}\right)^{\frac{1}{2}}. \end{aligned} \tag{25}$$

Moreover, for $t \in [0, \infty[$, we have

$$\begin{aligned} &|\mu(h_{a,y}(t), y)h'_{a,y}(t) - \mu(h_{a,y_{m_j}}(t), y_{m_j})h'_{a,y_{m_j}}(t)| \\ &= \left|\mu(h_{a,y}(t), y)\left(h'_{a,y}(t) - h'_{a,y_{m_j}}(t)\right) + h'_{a,y_{m_j}}(t)\left(\mu(h_{a,y}(t), y) - \mu(h_{a,y_{m_j}}(t), y_{m_j})\right)\right| \\ &\leq |\mu(h_{a,y}(t), y)| \cdot \left|h'_{a,y}(t) - h'_{a,y_{m_j}}(t)\right| \\ &\qquad + |h'_{a,y_{m_j}}(t)| \cdot \left|\mu(h_{a,y}(t), y) - \mu(h_{a,y_{m_j}}(t), y_{m_j})\right|. \end{aligned} \tag{26}$$

Combining the above equation with (24) and (25) implies

$$\begin{aligned} &|\mu(h_{a,y}(t), y)h'_{a,y}(t) - \mu(h_{a,y_{m_j}}(t), y_{m_j})h'_{a,y_{m_j}}(t)| \\ &\quad\leq \max_{y\in[y_{j-1},y_j],t\in[0,T_0]} |\mu(h_{a,y}(t), y)| \cdot M_{h'} \left|y_j - y_{j-1}\right| \\ &\qquad + \max_{y\in[y_{j-1},y_j],t\in[0,T_0]} |h'_{a,y_{m_j}}(t)| \cdot L\left|y_j - y_{j-1}\right|\left(M_h^2 + \frac{1}{4}\right)^{\frac{1}{2}} \\ &\quad=: C_{y_j,y_{j-1}}.\left|y_j - y_{j-1}\right|, \end{aligned} \tag{27}$$

with $C_{y_j,y_{j-1}}$ a positive constant determined by the size of the layer. Finally, for all $y \in [y_{j-1}, y_j]$, we deduce that

$$\begin{aligned} \left|\Lambda_a(y) - \Lambda_a(y_{m_j})\right| &\leq \int_0^{T_0} e^{-kt}\left|\mu(h_{a,y}(t), y)h'_{a,y}(t) - \mu(h_{a,y_{m_j}}(t), y_{m_j})h'_{a,y_{m_j}}(t)\right| \mathrm{d}t \\ &\leq C_{y_j,y_{j-1}}\left|y_j - y_{j-1}\right|\left(e^{-kT_0} - 1\right) =: C^{\Lambda}_{y_j,y_{j-1}}\left|y_j - y_{j-1}\right|. \end{aligned}$$

□

Assuming that Λ_a is constant over each layer leads to an error parameter which is linearly varying with the layers size and is independent of k. We fix y at the middle value y_{m_j}, compute $\Lambda_a(y_{m_j})$ and factor this term out of the integral over $[y_{j-1}, y_j]$. For n_y layers, we define $\hat{I}_{\Delta_1,n_y}(k)$ as the resulting approximation of $I^1_{\Delta_1}(k)$. Finally, one gets

$$\begin{aligned} \hat{I}_{\Delta_1,n_y}(k) = \sum_{j=1}^{n_y} \Bigg[&\Lambda_0(y_{m_j}) \int_{y_{j-1}}^{y_j} e^{ik\left(\sqrt{P(0,y)} + q_y y + s\right)} \mathrm{d}y \\ &- \Lambda_{1-y_{m_j}}(y_{m_j}) \int_{y_{j-1}}^{y_j} e^{ik\left(\sqrt{P(1-y,y)} + q_x(1-y) + q_y y + s\right)} \mathrm{d}y\Bigg]. \end{aligned} \tag{28}$$

The univariate phase functions in the remaining integrals only depend on y and have a similar form as those studied in the previous sections. Therefore, the same procedure applies and then it remains to apply the one-dimensional steepest descent method to each term. Finally, we end up with the evaluation of six steepest descent paths for each y-layer of the unit triangle.

6 Numerical results

In this section, we present some numerical experiments for the univariate case and triangular surfaces that show the accuracy and efficiency of the approach and formulas derived in the preceding sections.

6.1 The univariate case

For the univariate case, we numerically compute the integral in (8) for different spatial configurations and wave numbers. We choose the standard Matlab `integral` function with allowed absolute error of 10^{-16} as ground truth which has been deduced from a previous comparison with a brute force method based on the trapezoidal rule applied with an interval partitioning of resolution 10^{-6}. In the steepest descent method, the fast decaying integrals over complex paths are computed by means of the Gauss-Laguerre rule with 160 nodes. The configurations are chosen as follows

$$A = \begin{pmatrix} 0 & 0 \\ 2 & 0 \\ 0 & 2 \end{pmatrix}, \quad \mathbf{b} = \begin{pmatrix} 0 \\ -1 \\ 0 \end{pmatrix}, \quad \mathbf{r} = d \begin{pmatrix} \cos(\alpha) \\ \sin(\alpha) \\ 0 \end{pmatrix} + \begin{pmatrix} 0 \\ \sin(\alpha) \\ 0 \end{pmatrix}, \quad \boldsymbol{\theta} = \begin{pmatrix} 1 \\ 0 \\ 0 \end{pmatrix}, \tag{29}$$

where α corresponds to 100 uniformly distributed angles from $-\pi$ to π and d are 9 uniformly distributed distances from 0.2 to 3.8. The purpose of the second term in the determination of $\mathbf{r}$ is to bend the circles around $[-1, 1]$ to avoid an intersection with this interval. These configurations lead to surface integrals as in (5), from where we obtain the univariate integrals as in (8) and where we set $y = 0$, $a = 0$ and $b = 1$. Let us remind that in accordance with (8), the univariate integrals are denoted by $I(k, 0, 0, 1)$ in the cases treated here. Note that the bounds $a = 0$ and $b = 1$ in this notation are just a parametrisation and we actually integrate over the interval $[-1, 1]$ in the physical setting. The configuration together with the relative error between the Matlab `integral` (I_M) and steepest descent integral (I_{SD}) is displayed in Figure 4 (in $\log_{10}$-scale). We took different wave numbers $k \in \{100, 500, 3000, 5000\}$, and for each we computed the integral for all $100 \cdot 9 = 900$ scenarios described above and measured the CPU time. The experiment covers the three types of possible splitting point configurations, i.e. no splitting point or c_r or c_s being present on the integration interval, respectively.

For wavenumbers $k \in \{100, 500, 3000\}$, we achieve an average relative error (our method compared to Matlab) of less than 4.6×10^{-7} with a standard deviation of 1.4×10^{-11}. The maximum and minimum relative errors are 1.12×10^{-4} and 3.26×10^{-16}, respectively. The average absolute error is 2.2×10^{-8} with a standard deviation of 2.3×10^{-12}. The maximum and minimum absolute errors are 4.9×10^{-6} and 7.2×10^{-18}, respectively. For wave number $k = 5000$ we obtain the equal performance, except for 8 out of the 900 configurations, where the relative error is about 0.02 and the absolute error is about 3×10^{-4}. The accuracy for those cases can however be improved to less than 10^{-4} relative error by increasing the number of Gauss-Laguerre nodes to 1000. This shows that the method also works in this regime, but also underlines that some configurations require a careful adjustment of parameters. The average CPU time is reported in Figure 5. We observe that the computational cost grows linearly with respect to k for the Matlab `integral` function while the steepest descent method leads to a k-independent cost. For most configurations, the number of Gauss-Laguerre points could have been significantly reduced from 160 to about 40 with nearly no loss of accuracy. This provides one option to further accelerate the method.

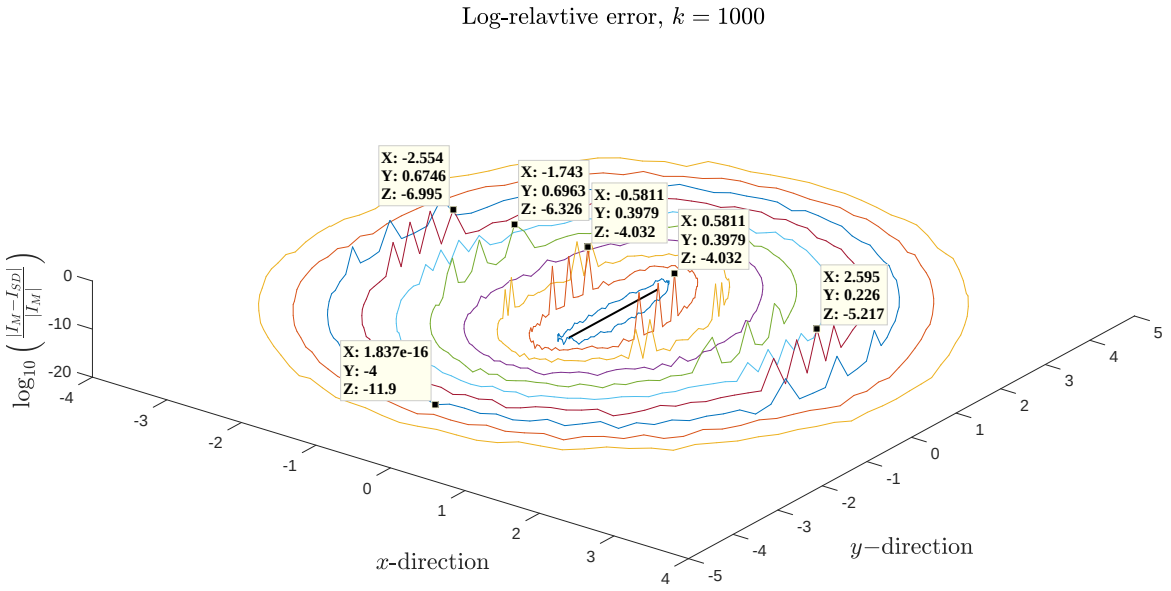

Figure 4: Relative error $|I_{\mathrm{M}} - I_{\mathrm{SD}}|/|I_{\mathrm{M}}|$ (in $\log_{10}$-scale) for the univariate integral $I(1000, 0, 0, 1)$ comparing our method (denoted by I_{SD}) with Matlab `integral` (given by I_{M}). The colored circle-like contours correspond to the different observation points, as described above, with the corresponding $\log_{10}$-relative error values as $z-$component. The black line segment describes the integration interval $[-1, 1]$.

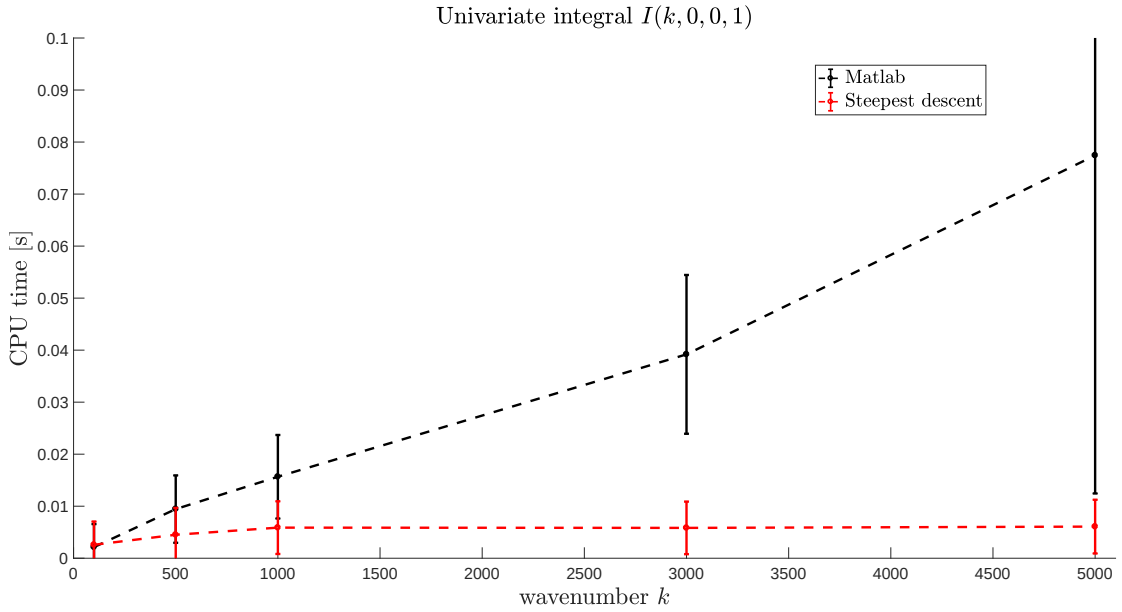

Figure 5: Average CPU time for the univariate integral $I(k,0,0,1)$ for 900 configurations as described and different wavenumbers $k = 100, 500, 1000, 3000, 5000$. The standard deviation is indicated by error bars; steepest descent (red); Matlab integral method (black).

To give some explicit values, we fixed $\alpha = 0$ and $d = 0.6$, which corresponds to a configuration with a splitting point, more precisely a stationary point in the middle of the interval. The numerical results for the corresponding univariate integrals are given in Table 3.

k	Steepest Descent	Matlab `integral` function	Rel. Error
100	$-0.0779921 - i0.1343569$	$-0.0779921 - i0.1343569$	1.44×10^{-15}
500	$0.0481076 - i0.529484$	$0.0481076 - i0.0529484$	1.15×10^{-14}
1000	$-0.0383622 - i0.0337473$	$-0.0383623 - i0.0337423$	9.71×10^{-5}
3000	$-0.0237740 - i0.0180741$	$-0.0237740 - i0.0180741$	5.11×10^{-7}
5000	$-0.01930278 - i0.01243698$	$-0.0193027 - i0.0124369$	1.31×10^{-8}

Table 3: Evaluation of $I(k,0,0,1)$ with the settings described above and different wave numbers k.

6.2 The case of triangular surfaces

For the surface integral in (5), we consider the same spatial configuration given in (29), where now α corresponds to 20 uniformly distributed angles from $-\pi$ to π while d is given by 9 uniformly sampled distances between 0.2 and 3.8. Due to computational feasibility, we reduced the number of angles compared to the 1-D case, and choose wavenumbers $k \leq 20$ to compare with Matlab `integral2`. The resolution in the y-direction in the implementation of (19) is set to 10^{-2} and the decaying integrals over the complex paths are evaluated by

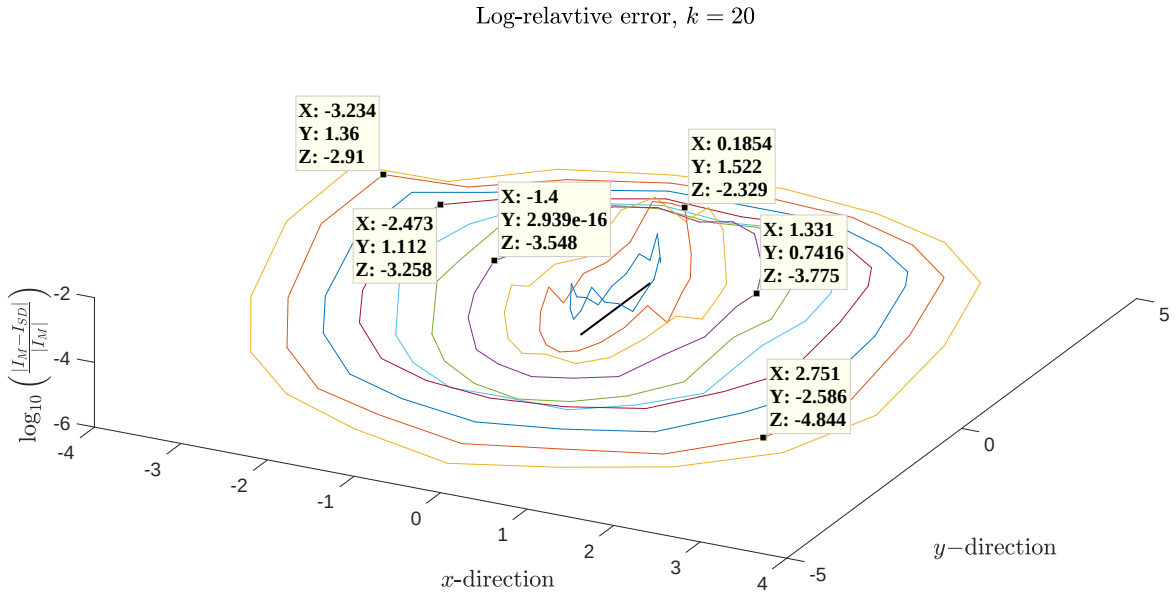

Figure 6: Relative error $|I_{\mathrm{M}} - I_{\mathrm{SD}}|/|I_{\mathrm{M}}|$ (in $\log_{10}$-scale) for the surface integral $I_\Delta(20)$ comparing our method (denoted by I_{SD}) with Matlab `integral2` (given by I_{M}). The colored circle-like contours correspond to the different observation points, as described above, with the corresponding $\log_{10}$-relative error values as $z-$component. The black line segment describes the orthogonal projection of the triangle surface onto the $xy-$plane.

the Gauss-Laguerre quadrature rule, taking 1000 nodes. The very large number of Gauss-Laguerre nodes is needed to show the performance in all configurations in the low wavenumber regime. At this point, we would like to mention that the computational costs of the overall method could be further reduced by an adaptive choice of parameters. The relative error in $\log_{10}$ scale for all configurations is reported in Figure 6 and the absolute error is reported in Figure 7. We achieve an average relative error (our method compared to Matlab) of less than 6.4×10^{-4} with a standard deviation of 4.5×10^{-11}. The maximum and minimum relative errors are 4.3×10^{-3} and 5.6×10^{-6}, respectively. The average absolute error is 1.4×10^{-7} with a standard deviation of 3.5×10^{-11}. The maximum and minimum absolute errors are 1.2×10^{-4} and 1.2×10^{-8}, respectively.

To prove the computational efficiency, we run the method for all $9 \cdot 20 = 180$ scenarios as described above for each wave number $k \in \{100, 500, 3000, 5000\}$, and measure the CPU time. For this evaluation, the number of Gauss-Laguerre nodes has been reduced to 160, which is justified by the fact that the results deviate by less than 9.2×10^{-6} and by 1.2×10^{-7} on average from those computed with 1000 nodes. The CPU time is reported for the two-dimensional steepest descent method only since the Matlab `integral2` function could not give reliable results for the wave numbers considered here, and a brute force approach took several minutes to compute reliable results in this setting. The corresponding results are given in Figure 8. We again observe the efficiency of the method with respect to k. From an inspection of the Matlab profiler outcome, it turns out that the increasing CPU time for large wavenumbers in Figure 8 is solely due to increasing computational costs of Matlab

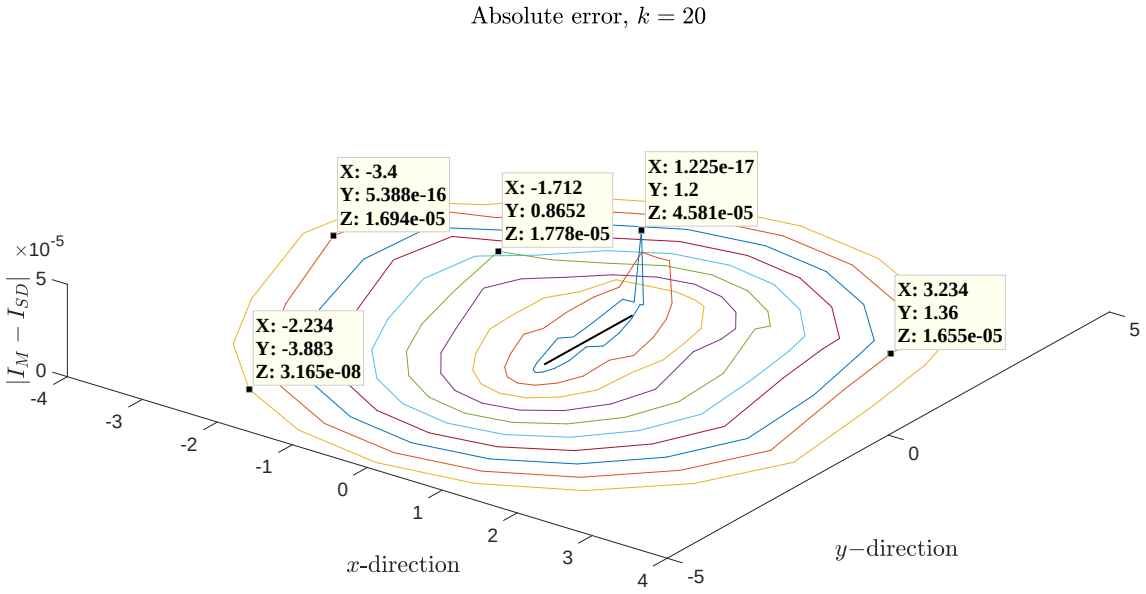

Figure 7: Error $|I_{\mathrm{M}} - I_{\mathrm{SD}}|$ for the surface integral $I_\Delta(20)$ comparing our method with Matlab `integral2`. The colored circle-like contours correspond to the different observation points, as described above, with the corresponding absolute error values as $z-$component. The black line segment describes the orthogonal projection of the triangle surface onto the $xy-$plane.

integration functions needed to handle integration about splitting points. In agreement with the theory, the computational cost of the pure steepest descent method is independent of the wavenumber.

Finally, to give some concrete results, let us fix $\alpha = 0$ and $d = 0.6$ and consider the results for $k \in \{5, 10, 20\}$. Again, the number of Gauss-Laguerre nodes was set to 1000 due to the low wavenumber regime. As comparison, we show integral values in Table (4) computed by the `integral2` function of Matlab with the paramater `AbsTol` being set to 10^{-16}. For the computations, we approximate the unit triangle by 10000 rectangular domains, each of which has a height equal to 10^{-4} and varying length equal to $1, 1 - 10^{-4}, 1 - 2 \times 10^{-4}, ..., 10^{-4}$, respectively, and compute the integral for each of these domains separately with `integral2`. We see a good agreement between the computed values.

k	Steepest Descent	Matlab `integral2` function	Rel. Error
5	$-0.0360801 - i0.1956997$	$-0.0354528 - i0.1958739$	3.3×10^{-3}
10	$0.0449510 + i0.0644971$	$0.0448265 + i0.0643822$	2.2×10^{-3}
20	$0.0172265 + i0.0308354$	$0.0172479 + i0.0308043$	1.2×10^{-3}

Table 4: Evaluation of $I_\Delta(k)$ with the settings described above.

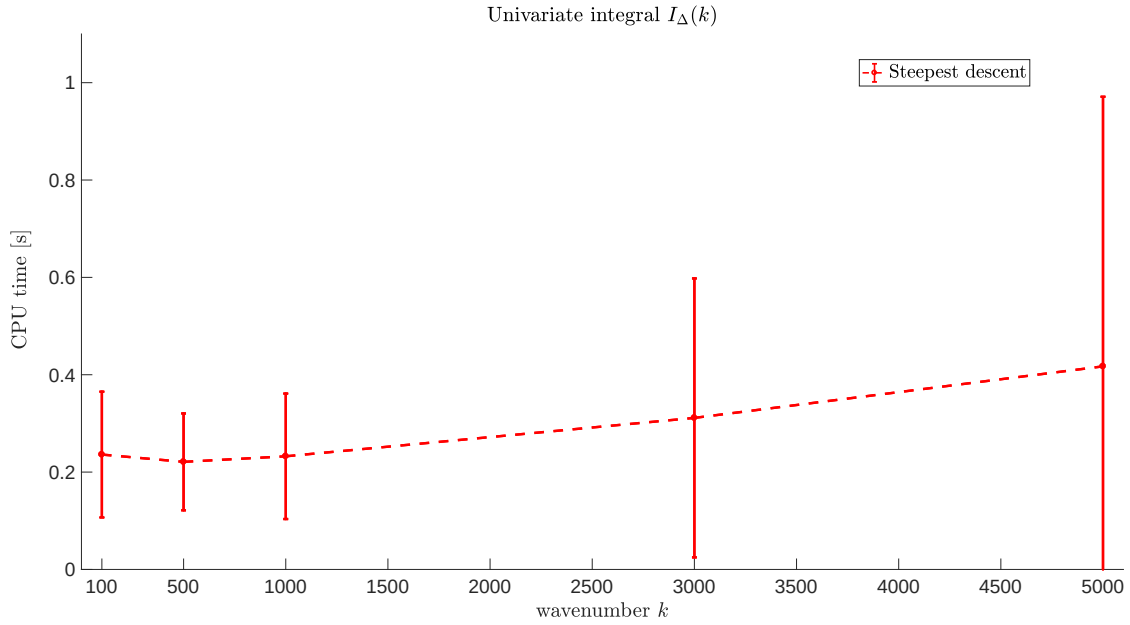

Figure 8: Average CPU time of steepest descent method for the surface integral $I_\Delta(k)$ for the 180 configurations as described beford and different wavenumbers $k = 100, 500, 1000, 3000, 5000$. The standard deviation is indicated by error bars

7 Conclusion

In this paper, we developed the application of the steepest descent method to the evaluation of the three-dimensional high-frequency acoustic single-layer operator over a surface Γ discretized by triangles. We derive formulas for both the splitting points and the admissible steepest descent paths, as well as some of their properties. We theoretically proof that the steepest descent method is applicable in every configuration as long the splitting points are treated accordingly. The integration scheme is next developed and numerical examples are reported to illustrate the efficiency and accuracy of the methodology, most particularly with respect to large wave numbers k. The approach should now be extended to other kinds of highly oscillatory integrals, and most particularly to the various standard surface potentials arising in three-dimensional acoustic and electromagnetic scattering.

References

[1] X. Antoine and M. Darbas. An introduction to operator preconditioning for the fast iterative integral equation solution of time-harmonic scattering problems. *Multiscale Science and Engineering*, 3:1–35, 2021.

[2] A. Asheim. A combined Filon/asymptotic quadrature method for highly oscillatory problems. *BIT Numerical Mathematics*, 48:425, 2008.

[3] A. Asheim. Applying the numerical method of steepest descent on multivariate oscillatory integrals in scattering theory. arXiv:1302.1019, 2013.

[4] A. Asheim. A remedy for the failure of the numerical steepest descent method on a class of oscillatory integrals. *BIT Numerical Mathematics*, 54(3):587–605, 2014.

[5] A. Asheim, A. Deaño, D. Huybrechs, and H. Wang. A Gaussian quadrature rule for oscillatory integrals on a bounded interval. *Discrete and Continuous Dynamical Systems-A*, 34(3):883–901, 2014.

[6] A. Asheim and D. Huybrechs. Asymptotic analysis of numerical steepest descent with path approximations. *Foundations of Computational Mathematics*, 10(6):647–671, 2010.

[7] O. Bruno and C. Geuzaine. An o (1) integration scheme for three-dimensional surface scattering problems. *Journal of Computational and Applied Mathematics*, 204(2):463–476, 2007.

[8] O. Bruno, C. Geuzaine, J. Monro Jr, and F. Reitich. Prescribed error tolerances within fixed computational times for scattering problems of arbitrarily high frequency: the convex case. *Philosophical Transactions of the Royal Society of London. Series A: Mathematical, Physical and Engineering Sciences*, 362(1816):629–645, 2004.

[9] S.N. Chandler-Wilde, I.G. Graham, S. Langdon, and E.A. Spence. Numerical-asymptotic boundary integral methods in high-frequency acoustic scattering. *Acta Numerica*, 21:89–305, 2012.

[10] W.C. Chew, E. Michielssen, J.M. Song, and J.M. Jin. *Fast and Efficient Algorithms in Computational Electromagnetics*. Artech House, 2001.

[11] A. Deaño, D. Huybrechs, and A. Iserles. *Computing Highly Oscillatory Integrals*, volume 155. SIAM, 2017.

[12] G. B. Folland. *Introduction to Partial Differential Equations*. Princeton University Press, 1995.

[13] J. Gao and A. Iserles. Error analysis of the extended Filon-type method for highly oscillatory integrals. *Research in Mathematical Sciences*, 4:21, 2017.

[14] J. Gao and A. Iserles. A generalization of Filon–Clenshaw–Curtis quadrature for highly oscillatory integrals. *BIT Numerical Mathematics*, 57:943–961, 2017.

[15] D. Huybrechs and S. Olver. *Highly oscillatory quadrature*, page 25–50. London Mathematical Society Lecture Note Series. Cambridge University Press, 2009.

[16] D. Huybrechs and S. Olver. Superinterpolation in highly oscillatory quadrature. *Foundations of Computational Mathematics*, 12:203–228, 2012.

[17] D. Huybrechs and S. Vandewalle. On the evaluation of highly oscillatory integrals by analytic continuation. *SIAM Journal on Numerical Analysis*, 44(3):1026–1048, 2006.

[18] D. Huybrechs and S. Vandewalle. The construction of cubature rules for multivariate highly oscillatory integrals. *Mathematics of Computation*, 76(260):1955–1980, 2007.

[19] A. Iserles and S. P. Nørsett. On quadrature methods for highly oscillatory integrals and their implementation. *BIT Numerical Mathematics*, 44(4):755–772, 2004.

[20] A. Iserles and S. P. Nørsett. Efficient quadrature of highly oscillatory integrals using derivatives. *Proceedings of the Royal Society of London Series A*, 461:1383–1399, 2005.

[21] A. Iserles and S. P. Nørsett. On the computation of highly oscillatory multivariate integrals with stationary points. *BIT Numerical Mathematics*, 46:549–566, 2006.

[22] A. Iserles and S. P. Nørsett. Quadrature methods for multivariate highly oscillatory integrals using derivatives. *Mathematics of Computation*, 46(255):1233–1258, 2006.

[23] A. Iserles and S. P. Nørsett. From high oscillation to rapid approximation III: multivariate expansions. *IMA Journal of Numerical Analysis*, 29(4):882–916, 2009.

[24] D. Levin. Fast integration of rapidly oscillatory functions. *Journal of Computational and Applied Mathematics*, 67(1):95–101, 1996.

[25] J.-C. Nédélec. *Acoustic and Electromagnetic Equations*. Applied Mathematical Sciences (144), New York, Springer-Verlag, 2001.

[26] Y. Wu, L. J. Jiang, and W. C. Chew. An efficient method for computing highly oscillatory physical optics integral. *Progress In Electromagnetics Research*, 127:211–257, 2012.

[27] Y. M. Wu and W. C. Chew. The modern high frequency methods for solving electromagnetic scattering problems. *Progress In Electromagnetics Research*, 156:63–82, 2016.

[28] Y. M. Wu, L. J. Jiang, and W. C. Chew. Computing highly oscillatory physical optics integral on the polygonal domain by an efficient numerical steepest descent path method. *Journal of Computational Physics*, 236:408 – 425, 2013.

[29] Y. M. Wu, L. J. Jiang, E. Wei, and W. C. Chew. The numerical steepest descent path method for calculating physical optics integrals on smooth conducting quadratic surfaces. *IEEE Transactions on Antennas and Propagation*, 61(8):4183–4193, 2013.

[30] Y. M. Wu and S. J. Teng. Frequency-independent approach to calculate physical optics radiations with the quadratic concave phase variations. *Journal of Computational Physics*, 324:44–61, 2016.

[31] S. Xiang. On the Filon and Levin methods for highly oscillatory integral. *Journal of Computational and Applied Mathematics*, 208(2):434–439, 2007.

[32] Jun Zhang, Wen Ming Yu, Xiao Yang Zhou, and Tie Jun Cui. Efficient evaluation of the physical-optics integrals for conducting surfaces using the uniform stationary phase method. *IEEE Transactions on Antennas and Propagation*, 60(5):2398–2408, 2012.

[33] L. Zhao and C. Huang. An adaptive Filon-type method for oscillatory integrals without stationary points. *Numerical Algorithms*, 75(3):753–775, 2017.